Nuclear Quadrupole Interaction at $^{187}W(\beta^-)^{187}Re$ in Tungsten Compounds*

Pit Schmidt**, Torsten Soldner***, Wolfgang Tröger, Xinbo Ni‡, Tilman Butz, and Peter Blaha[a]

[a] Institut für Technische Elektrochemie, Technische Universität Wien, Getreidemarkt 9/158, A-1030 Wien

Z. Naturforsch. **53a,** 323–339 (1998); received January 26, 1998

The nuclear quadrupole interaction at $^{187}W(\beta^-)^{187}Re$ was determined by time differential perturbed angular correlation inWC, WS_2, WSe_2, WSi_2, and $CaWO_4$ to be (at 300 K): ν_Q = 335.9(2), 1094.9(1), 1031.6(1), 1131.5(1), and 1085.9(1) MHz, respectively. The asymmetry parameter η was zero in all cases. For WSe_2 and $CaWO_4$ the temperature dependence of the nculear quadrupole interaction was determined between 300 K and about 900 K. Ab initio calculations of electric field gradients, using the WIEN95-code, were carried out for WC, WS_2, WSe_2, and WSi_2 at W-sites and Re-impurities, and for $CaWO_4$ at W-sites. Good agreement with experimental data was found.

1. Introduction

Tungsten and tungsten compounds play an important role in industrial applications. Examples are W-filaments in bulbs, WC with 5–10% Co exhibiting extraordinary hardness ("WIDIA"), or W-based catalysts [1, 2]. Multilayers consisting of W and Si are used as X-ray monochromators [3]. W also plays a role in micro-organisms. Thermophilic archaea, e.g., use W-enzymes for methanogenesis [4, 5, 6]. Hence, it would be desirable to have a hyperfine spectroscopic tool to investigate the nuclear quadrupole interaction in such systems. Classical techniques like nuclear magnetic resonance or nuclear quadrupole resonance are hampered by the lack of suitable nuclei (the naturally occurring isotopes have either a nuclear spin $I = 0$ or $I = 1/2$ groundstate). Mössbauer spectroscopy on ^{182}W has a first excited state with $I = 2$ but suffers from poor energy resolution. An interesting alternative is offered by time differential perturbed angular correlation (TDPAC) of γ-rays from ^{187}W ($T_{1/2}$ = 24 h) which feeds the 479.5 keV – 72 keV γ-γ-cascade in ^{187}Re via β^--decay. The disadvantage is that the nuclear quadrupole interaction (NQI) is determined at ^{187}Re, presumably on a W-lattice site, and not directly at a W-isotope. There are, however, important advantages counterbalancing this drawback:

(i) TDPAC is extremly sensitive, about 10^{10} atoms suffice; this is particularly important for biophysical applications.
(ii) The energy or frequency resolution of this TDPAC isotope is excellent due to the very long halflife of the intermediate (206.2 keV) excited state ($\tau_{1/2}$ = 555.3 ns).
(iii) The anisotropy of the γ-γ-cascade is large: $A_{22} = -13.1\%$ [7].
(iv) The nuclear quadrupole moment of the 206.2 keV state is large: Q = 3.04(5) b [7].

Despite these most favourable nuclear properties, applications with ^{187}W-TDPAC were rather scarce [8, 9, 10] for the following reasons:

(i) Due to the large quadrupole moment, the NQI-frequencies are frequently rather high and require subnanosecond timing, i.e. BaF_2-scintillators.
(ii) The intermediate excited state has $I = 9/2$, which leads to a multitude of up to 10 lines for non-axial symmetry in a Fourier transformed TDPAC-spectrum.
(iii) The stop-γenergy of 72 keV is just heigh enough to produce prompt K-X-rays after K-edge absorption; this X-ray admixture reduces the effective anisotropy drastically; this effect is more severe with BaF_2-scintillators compared to NaI(Tl).

---

* Presented at the XIVth International Symposium on Nuclear Quadrupole Interactions, Pisa, Italy, July 20–25, 1997.
** Present address: Fachbereich Physik, Johannes-Gutenberg-Universität Mainz, 55099 Mainz, Germany.
*** Present address: Physik-Department E21, TU München, 85748 Garching, Germany.
‡ Present address: Shanghai Institute of Nuclear Research, China.

Reprint requests to Dr. W. Tröger; Fax: 49-0341-9732-729.

0932-0784 / 98 / 0600-0323 $ 06.00 © – Verlag der Zeitschrift für Naturforschung, D-72027 Tübingen

Dieses Werk wurde im Jahr 2013 vom Verlag Zeitschrift für Naturforschung in Zusammenarbeit mit der Max-Planck-Gesellschaft zur Förderung der Wissenschaften e.V. digitalisiert und unter folgender Lizenz veröffentlicht: Creative Commons Namensnennung-Keine Bearbeitung 3.0 Deutschland Lizenz.

This work has been digitalized and published in 2013 by Verlag Zeitschrift für Naturforschung in cooperation with the Max Planck Society for the Advancement of Science under a Creative Commons Attribution-NoDerivs 3.0 Germany License.

Zum 01.01.2015 ist eine Anpassung der Lizenzbedingungen (Entfall der Creative Commons Lizenzbedingung „Keine Bearbeitung") beabsichtigt, um eine Nachnutzung auch im Rahmen zukünftiger wissenschaftlicher Nutzungsformen zu ermöglichen.

On 01.01.2015 it is planned to change the License Conditions (the removal of the Creative Commons License condition "no derivative works"). This is to allow reuse in the area of future scientific usage.

Therefore ^{187}W is not considered a very suitable isotope among TDPAC-spectroscopists. Despite these drawbacks we initiated a study with this nuclear probe in several W-compounds using a high efficiency 6-detector TDPAC-camera [11]. In this way, $10^8 \ldots 10^9$ coincidences could be recorded per spectrum in total. Moreover, a new method of data analysis, namely cross correlation [12], was found to be rather useful to cope with the multiline problem due to $I = 9/2$. With these hard- and software improvements, ^{187}W-TDPAC spectroscopy turns out to be rather promising, as demonstrated in this paper.

2. TDPAC and Nuclear Quadrupole Interaction

TDPAC usually requires a γ-γ-cascade. Due to angular momentum conservation the observation of γ_1 in a certain direction produces an aligned subensemble of nuclei whose subsequent emission of γ_2 is anisotropic. Hence, the coincidence countrate between γ_1 and γ_2 is anisotropic in general, whereas the individual emission characteristics of γ_1 and γ_2 are isotropic:

$$W(\boldsymbol{k}_1, \boldsymbol{k}_2) = \sum_k A_k(\gamma_1)\, A_k(\gamma_2)\, P_k(\cos\theta). \qquad (1)$$

Here, $\boldsymbol{k}_1$ and $\boldsymbol{k}_2$ are the emission directions of γ_1 and γ_2 with θ denoting the angle between them. The sum runs over even integers due to parity conservation of the electromagnetic interaction. Usually, $k = 0, 2$ is sufficient. $A_k(\gamma_1)$ and $A_k(\gamma_2)$ are coefficients depending on the nuclear spins involved in the transition and on mixing ratios for mixed multipolarities. In the case of the 479.5 keV – 72 keV cascade in ^{187}Re we have: $A_2(\gamma_1)A_2(\gamma_2) \equiv A_{22} = -0.131$, $A_{44} = 0$. $P_k(\cos\theta)$ is a Legendre polynomial. If the nucleus in the intermediate excited state is subjected to extranuclear fields – in our case it interacts via its nuclear quadrupole moment with an electric field gradient (EFG) – the angular correlation of (1) is modified:

$$W(\boldsymbol{k}_1, \boldsymbol{k}_2, t) = e^{-t/\tau_N} \sum_k A_{kk}\, G_{kk}(t)\, P_k(\cos\theta). \qquad (2)$$

This time dependent angular correlation applies to random powder samples. The function $G_{kk}(t)$ is called perturbation function and contains all information about the NQI. The exponential factor accounts for the fact that the coincidence probability between γ_1 and γ_2 with a time-lag t between them decreases with the lifetime τ_N of the intermediate excited state.

In the case of axial symmetry of the EFG-tensor, i.e. $\eta = (V_{xx} - V_{yy})/V_{zz} = 0$, we have for $I = 9/2$

$$G_{22}(t) = \frac{1}{5} + \frac{29}{165}\cos\omega t + \frac{14}{165}\cos 2\omega t + \frac{3}{11}\cos 3\omega t + \frac{8}{55}\cos 4\omega t + \frac{14}{165}\cos 5\omega t + \frac{2}{55}\cos 7\omega t \qquad (3)$$

with $\omega = eQV_{zz}/24\,\hbar$ and eQ denoting the nuclear quadrupole moment of the intermediate excited state. V_{zz} is the largest component of the EFG-Tensor. Frequently, the NQI-frequency is quoted as $\nu_Q = eQV_{zz}/h = 12\ \omega/\pi$.

Summing up, the coincidence countrate of (2) is periodically modulated by the perturbation function of (3). The larger τ_N ("exploration time"), the more oscillations are observable and, hence, the better the frequency resolution.

3. Spectrometer and Data Analysis

We used the 6-detector TDPAC-camera [11] equipped with conically capped BaF_2-scintillators. In this way, 6 coincidence spectra at $\theta = 180°$ and 24 coincidence spectra at $\theta = 90°$ can be recorded simultaneously. Because we allocated 1024 channels per subgroup (i.e., we used a 32 K multichannel analyzer) and because we anticipated high frequencies, we used approximately 1 ns per channel. In this way, only about 750 ns could be monitored which corresponds to about 1.5 halflifes of ^{187}W only. Usually five to ten halflifes are observable before the signal to noise ratio becomes excessively small. This, however, would have required 4 K per subgroup or a 128 K multichannel analyzer which became available only recently. Hence, the frequency resolution could be improved by a factor of 4 easily compared to what is presented below. The experimental time resolution for the 479.5 keV – 72 keV cascade was about 850 ps.

The data analysis was performed as follows: First, the uncorrelated background of accidental coincidences was determined from the spectral region of $t < 0$ and subtracted from the raw data. Next, all spectra were shifted to a common origin of time ($t = 0$). The huge prompt contribution in each subgroup served for that purpose. Finally, the following ratio was formed:

$$R(t) = 2\,\frac{W(180°) - W(90°)}{W(180°) + 2\,W(90°)} \qquad (4)$$

with

$$W(180°) = \sqrt[6]{W_{13}W_{31}W_{24}W_{42}W_{56}W_{65}},$$

$$W(90°) = \sqrt[24]{P}, P = \prod_{i,j=1;i\neq j}^{6} W_{ij}$$

$$\text{without } W_{13}, W_{31}, W_{24}, W_{42}, W_{56}, W_{65}. \quad (5)$$

Here, W_{ij} denotes the coincidences between detectors i (start) and j (stop). By forming this ratio, the exponential decay factors cancel and the detector efficiences cancel to first order. Restricting to random powder samples and $k = 2$ (this is true in the present case) we have

$$R(t) = A_{22}\, G_{22}(t). \quad (6)$$

$R(t)$ is called the "time spectrum". Its cosine transform yields a comb of equidistant lines (for asymmetry parameter zero) with intensities of (3).

The following modifications of (6) are necessary, when actually fitting time spectra:

(i) A_{22} is reduced because of solid angle correction factors (the detector averages over the acceptance angle) and in the present case due to the X-ray admixture in the stop channel. Hence, A_{22} is treated as a free parameter.

(ii) The finite time resolution of the spectrometer leads to a progressive suppression of higher frequencies, which can be approximated by the following factor multiplying the cosine terms in (3):

$$e^{-0.09\,\tau_{FWHM}^2\, n^2\omega^2}, \quad n = 1,\ldots,7, \quad (7)$$

where τ_{FWHM} denotes the full width at half maximum of the time resolution function (assumed Gaussian).

(iii) A static inhomogeneous distribution of frequencies ω (assumed Lorentzian) leads to an additional time dependent factor which causes a damping of the oscillations (or, equivalently, a line-broadening of the Fourier-transformed time spectrum):

$$e^{-\delta n\omega t}, \quad n = 1,\ldots,7, \quad (8)$$

with δ being the half width at half maximum of the frequency distribution function.

In practice, a time independent baseline shift is also fitted and treated as a free fitting parameter.

In order to obtain a first good guess for the fitting parameter ω we performed a cross-correlation analysis, as described in [12].

4. Sample Preparation

WC was purchased from Fluka. It crystallizes in the space group $P\bar{6}m2$[1] with lattice constants $a = 2.9065$ Å and $c = 2.8366$ Å. There is one formula unit per unit cell [13].

Single crystals of WS_2 and WSe_2 were prepared by vapour transport and generously provided by Prof. F. Lévy, EPF Laussane, and Prof. E. Bucher, University of Konstanz. Both layered dichalcogenides crystallize in the space group $P6_3/mmc$[2] with lattice constants $a = 3.1532$ Å, $c = 12.329$ Å and $a = 3.2882$ Å, $c = 12.96$ Å, respectively. There are two formula units per unit cell [14, 15].

WSi_2 was purchased from Johnson Matthey. It crystallizes in the space group $I4/mmm$[3] with lattice constants $a = 3.2718$ Å and $c = 7.8403$ Å. There are two formula units per unit cell [16].

$CaWO_4$ was generously provided by Prof. G. Völkel and Dr. J. Simon, University of Leipzig, in the form of small single crystals. It crystallizes in the space group $I4_1/a$[4] with lattice constants $a = 5.2429$ Å and $c = 11.3737$ Å. There are 4 formula units per unit cell [17].

We expect axial symmetry for the EFG-Tensor in all cases because there is a threefold rotation axis in WC, WS_2, and WSe_2, a fourfold rotation axis in WSi_2, and a fourfold inversion axis in $CaWO_4$.

All samples were neutron irradiated at the Forschungsreaktor München (FRM) at a thermal neutron flux of about $2 \cdot 10^{13}$ n/(cm^{2}s) for about 10 min to 2 hours. In principle, we should expect radiation damage as a consequence of prompt γ-deexicitation ($E_{max} = 5.5$ MeV) following the neutron capture. The recoil energy of $E_{recoil,max} = 90$ eV should be more than sufficient to produce near neigbour vacancies. However, we did not observe any indication for radiation damage in any of our samples. Thermal annealing of WS_2 after irradiation at 800 °C for 2 h did not produce any noticeable effect. Measurements at elevated temperatures up to 764 K for WSe_2 and 911 K for $CaWO_4$ did not yield sharper lines or an increase in effective anisotropy A_{22}. Hence, we believe that in all cases light displaced neighbouring at-

[1] W at (0, 0, 0) and C at $(\frac{2}{3}, \frac{1}{3}, \frac{1}{2})$.

[2] W at $(\frac{1}{3}, \frac{2}{3}, \frac{1}{4})$, S and Se at $(\frac{1}{3}, \frac{2}{3}, u)$, with $u = 0.6225$ for S and $u = 0.6211$ for Se, respectively.

[3] W at (0, 0, 0) and Si at (0, 0, 0.3345).

[4] Ca at $(0, \frac{1}{4}, \frac{5}{8})$, W at $(0, \frac{1}{4}, \frac{1}{8})$, and O at (0.1507, 0.0086, 0.2106).

oms are mobile enough at 433 K (the temperature during irradiation) to recombine with vacancies, i.e., the radiation damage is already annealed before we started the TDPAC measurements. Therefore all samples were used "as irradiated". Because of the relatively short halflife of ^{187}W (24 h) we irradiated 4 samples with weight ratios 1:2:4:8 simultaneously and changed samples every 24 h. The total data collection time per spectrum was 4–5 days.

In order to minimize selfabsorption in the sample, we used very small specimens (0.1–0.4 mg) only, unless stated otherwise. No isotope enrichment was necessary.

5. Results

5.1. TDPAC-Experiments

5.1.1. WC

The time spectrum for WC at room temperature together with its cosine transform is shown in Figure 1. The typical $I = 9/2$ random powder pattern for axial symmetry is immediately recognizeable. There is some damping of the oscillation amplitude. Moreover, a dispersive-like distortion is visible around 550 Mrad/s which is a consequence of a mismatch of the anode signal to the constant fraction triggers, as verified with a 5 Gsamples/s digital oscilloscope in the averaging mode. There is also a slightly increasing baseline for the first 100 ns which leads to the low-frequency intensity in the cosine transformed spectrum. Finally, there is a sloping baseline in the range 100 ns–750 ns. The latter two effects could be eliminated totally by the use of a veto-logic which prevents triple and higher multiple coincidences. However, both baseline problems have no influence on the determination of the NQI-parameters. A least squares fitting analysis yielded $\omega =$ 87.94(5) Mrad/s, a Lorentzian damping of $\delta = 1.36(6)\%$ and an effective anisotropy of $A_{22}^{\text{eff}} = -2.25(6)\%$. A total of $1.6 \cdot 10^9$ coincidences was recorded for this spectrum.

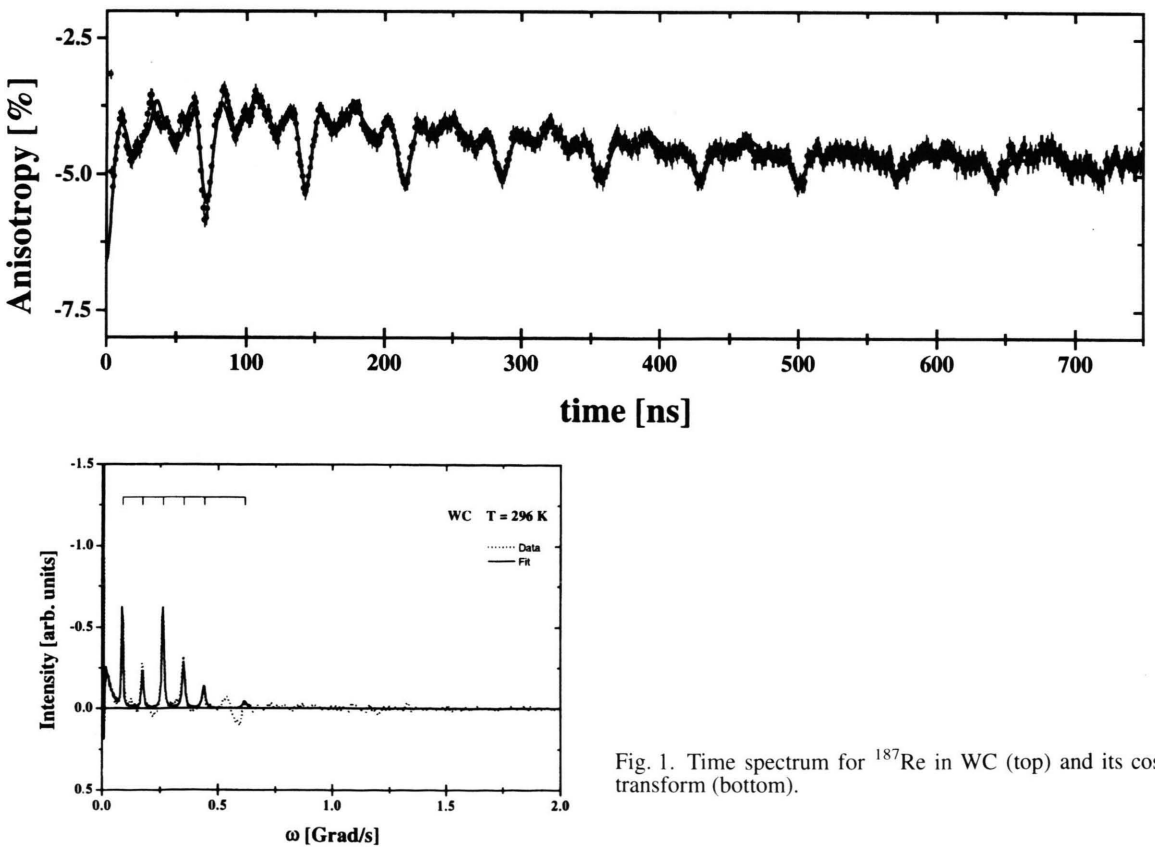

Fig. 1. Time spectrum for ^{187}Re in WC (top) and its cosine transform (bottom).

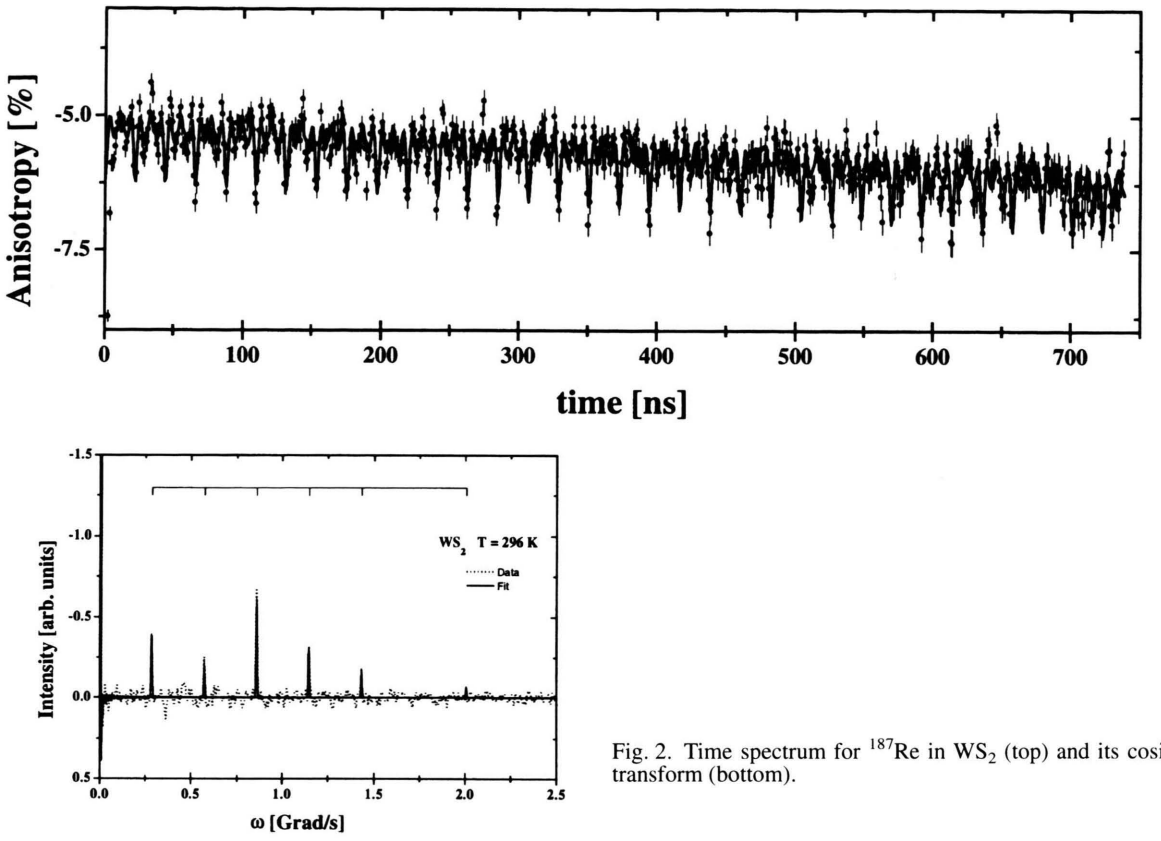

Fig. 2. Time spectrum for ^{187}Re in WS_2 (top) and its cosine transform (bottom).

5.1.2. WS_2

The time spectrum for WS_2 at room temperature together with its cosine transform is shown in Figure 2. It is immediately clear that the NQI is much higher compared to the case of WC. There are still problems with the very slightly sloping baseline and electronic distortions in the first 50 ns of the time spectrum. In fact, these distortions were modelled and subtracted from the time spectrum prior to the cosine transformation. All harmonics but 7ω are clearly visible despite the high fundamental frequency. This is clearly due to the good time resolution of BaF_2-scintillators. A least squares fitting analysis yielded $\omega = 286.64(3)$ Mrad/s and an effective anisotropy of $A_{22}^{\text{eff}} = -1.21(3)\%$. No Lorentzian damping was required: in fact, the fit yielded a slightly negative value for δ when treated as a free parameter, which is unphysical. A total of $5 \cdot 10^8$ coincidences was recorded for this spectrum.

5.1.3. WSe_2

The time spectrum for WSe_2 at room temperature together with its cosine transform is shown in Figure 3. The spectrum closely resembles that for WS_2. There are no more baseline problems. They all could be eliminated by a triple coincidence veto. Electronic distortions were greatly reduced, but are corrected for prior to the cosine transformation. A least squares fitting analysis yielded $\omega = 270.08(3)$ Mrad/s, a Lorentzian damping of $\delta = 0.15(2)\%$ and an effective anisotropy of $A_{22}^{\text{eff}} = -1.9(1)\%$. A total of $3.8 \cdot 10^8$ coincidences was recorded for this spectrum.

We subsequently performed measurements at elevated temperatures up to 764 K in sealed quartz ampoules filled with inert gas. Typically $8 \cdot 10^7$ coincidences were sufficient to extract the NQI-parameters with sufficient accuracy. The time spectra for various temperatures (first 300 ns are shown only) and their cosine transforms are shown in Figure 4. Apparently the signal is almost lost at 764 K, much below the reported stability range for WSe_2 [18]. We cannot exclude the influence of oxidation due to residual oxygen in our closed quartz ampoules. Nevertheless, this observation is in keeping with the fact that our early attempts to anneal WSe_2 after neutron irradiation at 800 °C for 2 hours led to a complete absence

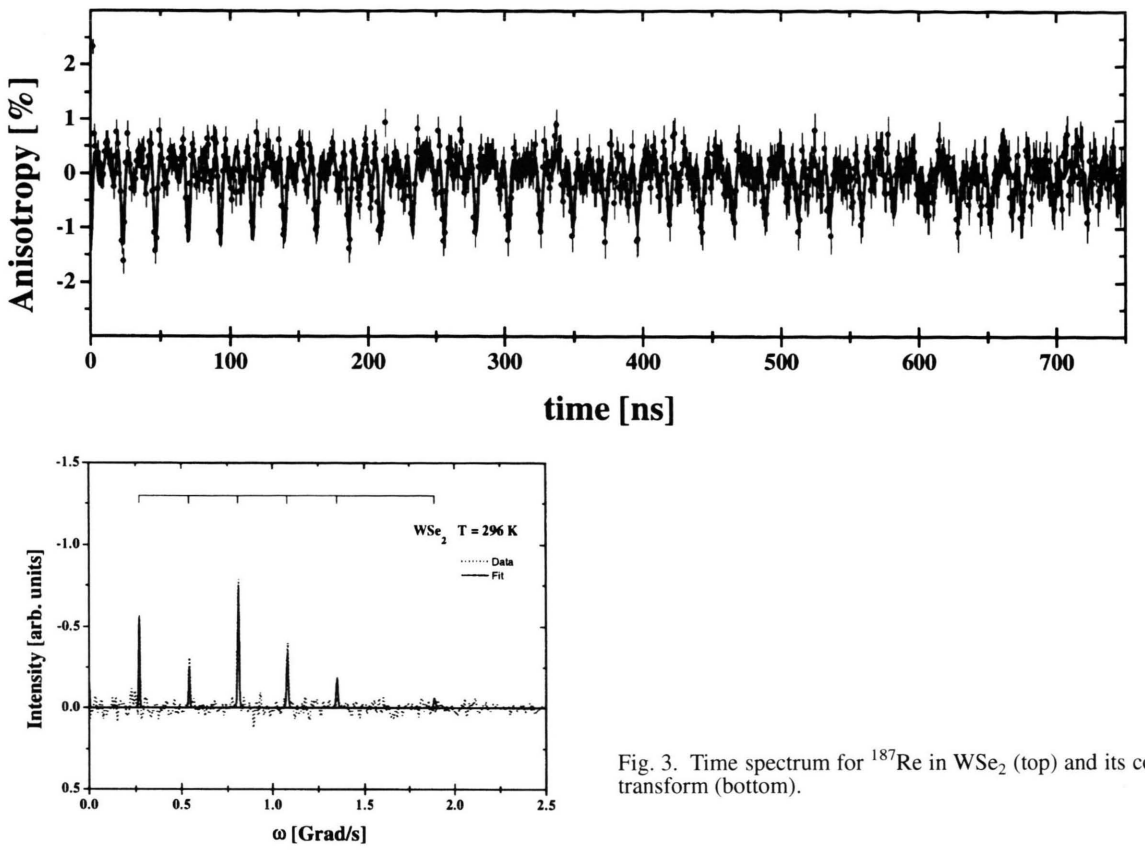

Fig. 3. Time spectrum for ^{187}Re in WSe_2 (top) and its cosine transform (bottom).

of a NQI-signal, whereas the same procedure applied to WS_2 had no deteriorating effect (it also did not improve the signal intensity or linewidth). Hence, WSe_2 is less stable and possibly more susceptible to oxidation than WS_2.

A further remark is necessary concerning line intensities in Figs. 3 and 4. For all experiments we used one single crystal of WSe_2, orientated roughly along the body diagonal of the cubic detector arrangement, i.e. along (111). For this geometry, the intensities differ slightly from those of the powder pattern. We have

$$G_{22}(t) = 0 + \frac{1}{6}\cos\omega t + \frac{14}{99}\cos 2\omega t + \frac{23}{66}\cos 3\omega t + \frac{8}{33}\cos 4\omega t + \frac{7}{99}\cos 5\omega t + \frac{1}{33}\cos 7\omega t, \quad (9)$$

which should be compared with (3) for random powder samples. The difference in the time independent term is irrelevant because it was treated as an adjustable parameter for technical reasons, anyway. Relevant differences exist for 2ω and 4ω. The quality of the fits, however, did not improve when using (9) instead of (3). This is most likely due to the fact that the crystal orientation within the furnace was not accurately along (111) and might even have changed during the data collection. In Figs. 3 and 4 the fits with random powder intensities according to (3) are shown. There is practically no difference in the fitted frequencies using either (3) or (9). All fit results are summarized in Table 1. The temperature dependence of ν_Q for WSe_2 is shown in Fig. 5 together with that of WS_2 taken from [10]. In addition, data for $CaWO_4$ are shown (see below). The solide lines represent least squares fits to the data points of the function

$$\nu_Q(T) = \nu_Q(0)(1 - \alpha T^\gamma). \quad (10)$$

The fit for $\nu_Q(0)$, α, and γ are listed in Table 2.

5.1.4. WSi_2

The time spectrum for WSi_2 at room temperature together with its cosine transform is shown in Figure 6.

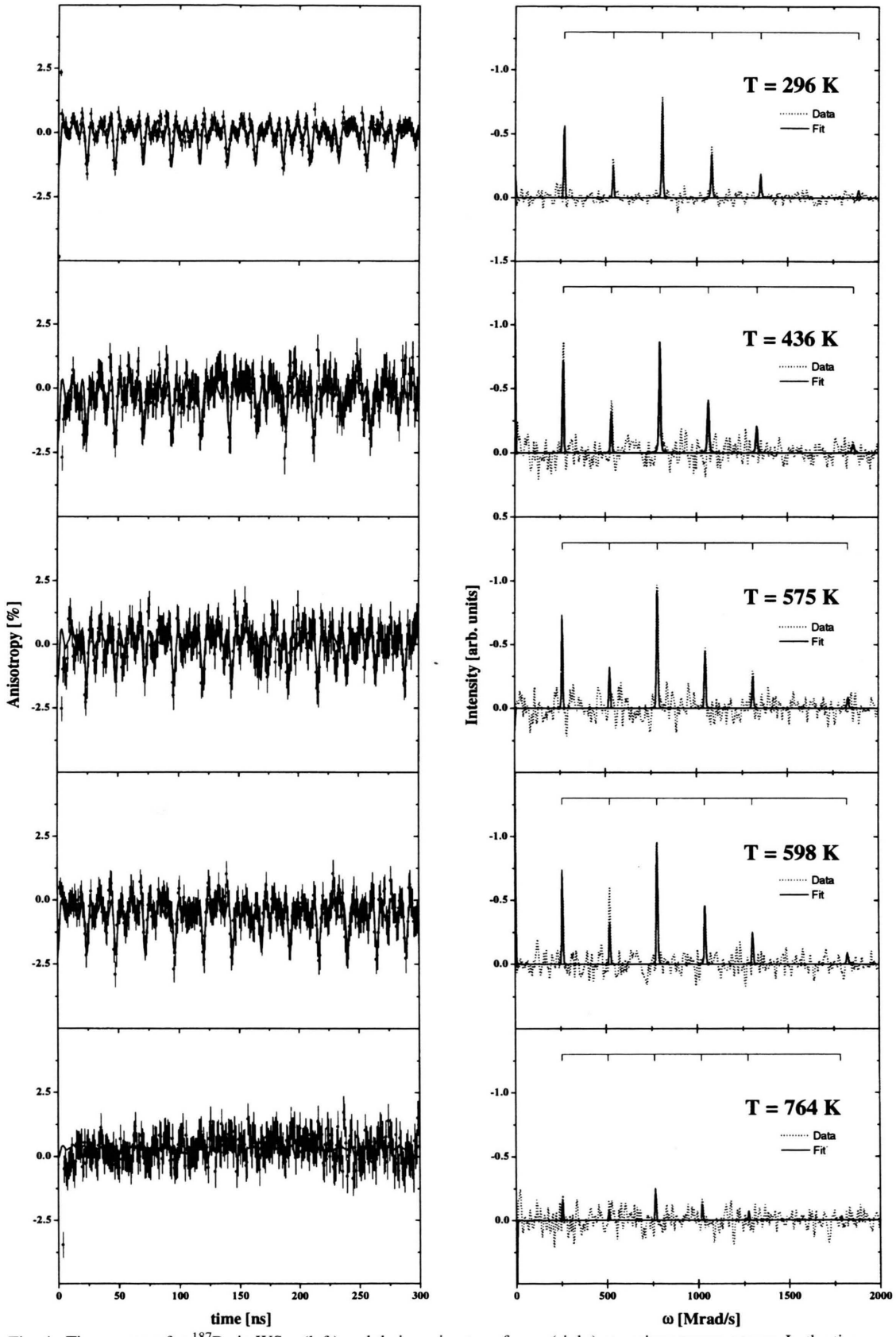

Fig. 4. Time spectra for ^{187}Re in WSe_2 (left) and their cosine transforms (right) at various temperatures. In the time spectra the first 300 ns are shown only.

Table 1. Summary of fit results for ^{187}Re in WSe_2 at various temperatures.

T [K]	ω_1 [Mrad/s]	Amplitude [%]	δ [%]	η	ν_Q [MHz]	$\lvert V_{zz}\rvert$ [10^{21} V/m^2]
296	270.08(3)	–1.9(1)	0.15(2)	0	1031.6(1)	14.0(2)
435	266.27(7)	–2.6(1)	0.24(2)	0	1017.1(3)	13.8(2)
575	262.03(5)	–2.3(1)	0.11(3)	0	1000.9(2)	13.6(2)
598	261.19(4)	–2.2(1)	0.09(2)	0	997.7(2)	13.6(2)
764	255.45(9)	–0.5(1)	0.00(2)	0	975.7(5)	13.3(2)

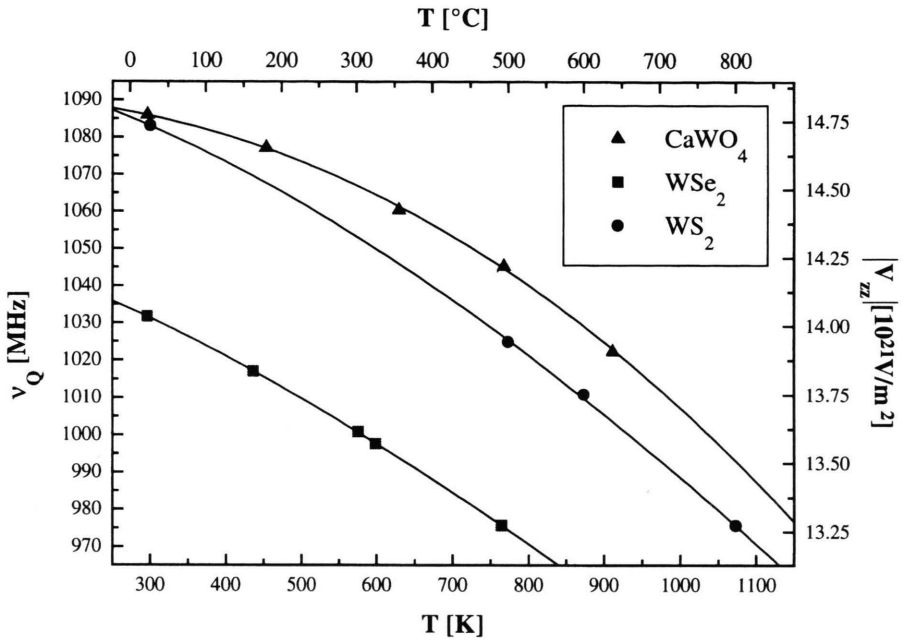

Fig. 5. ν_Q vs. temperature for $CaWO_4$, WSe_2, and WS_2. The data for WS_2 are taken from [10]. The V_{zz}-values were calculated using $Q = 3.04$ b [7].

Table 2. Fit results for ν_Q, α, and γ according to (10) for the temperature dependence of ν_Q for WS_2, WSe_2, and $CaWO_4$.

	$\nu_Q(0)$ [MHz]	α [10^{-4}]	γ
WS_2	1100(3)	20(10)	1.6(1)
WSe_2	1052(1)	66(2)	1.40(3)
$CaWO_4$	1092(2)	0.2(2)	2.2(1)

Although the characteristic pattern for $I = 9/2$ is clearly visible, the spectrum suffers from the rather low anisotropy $A_{22}^{\text{eff}} = -0.81(8)\%$ and relatively large Lorentzian damping of $\delta = 0.9(1)\%$, despite the high statistical accuracy ($1.4 \cdot 10^9$ coincidences). This is not due to parasitic activities due to neutron capture of Si which totally decayed prior to the start of our TDPAC-experiments, but presumably reflects the quality of the starting material. However, $\omega = 296.22(3)$ Mrad/s can be determined without problems.

5.1.5. $CaWO_4$

The time spectrum for $CaWO_4$ at room temperature together with its cosine transform is shown in Figure 7. There are no technical problems with the baseline and electronic distortions are very small. A least squares fitting analysis yielded $\omega = 284.30(2)$ Mrad/s, $A_{22}^{\text{eff}} = -1.19(3)\%$, and no Lorentzian damping was required at all. A total of $8.1 \cdot 10^8$ coincidences was recorded for this spectrum. We subsequently performed measurements up to 511 K. The time spectra (only the first 300 ns are shown) and their cosine transforms are shown in Figure 8 at various temperatures. We recorded $0.7 \ldots 1.4 \cdot 10^8$ coincidences per spectrum. The small amplitude of the signal at 767 K has a simple explanation: This was in fact the last measurement, and instead of a few very small single crystals we used all material of the previous experiments such that selfabsorption in the sample was severe. The origin of the sloping baseline in the spectrum

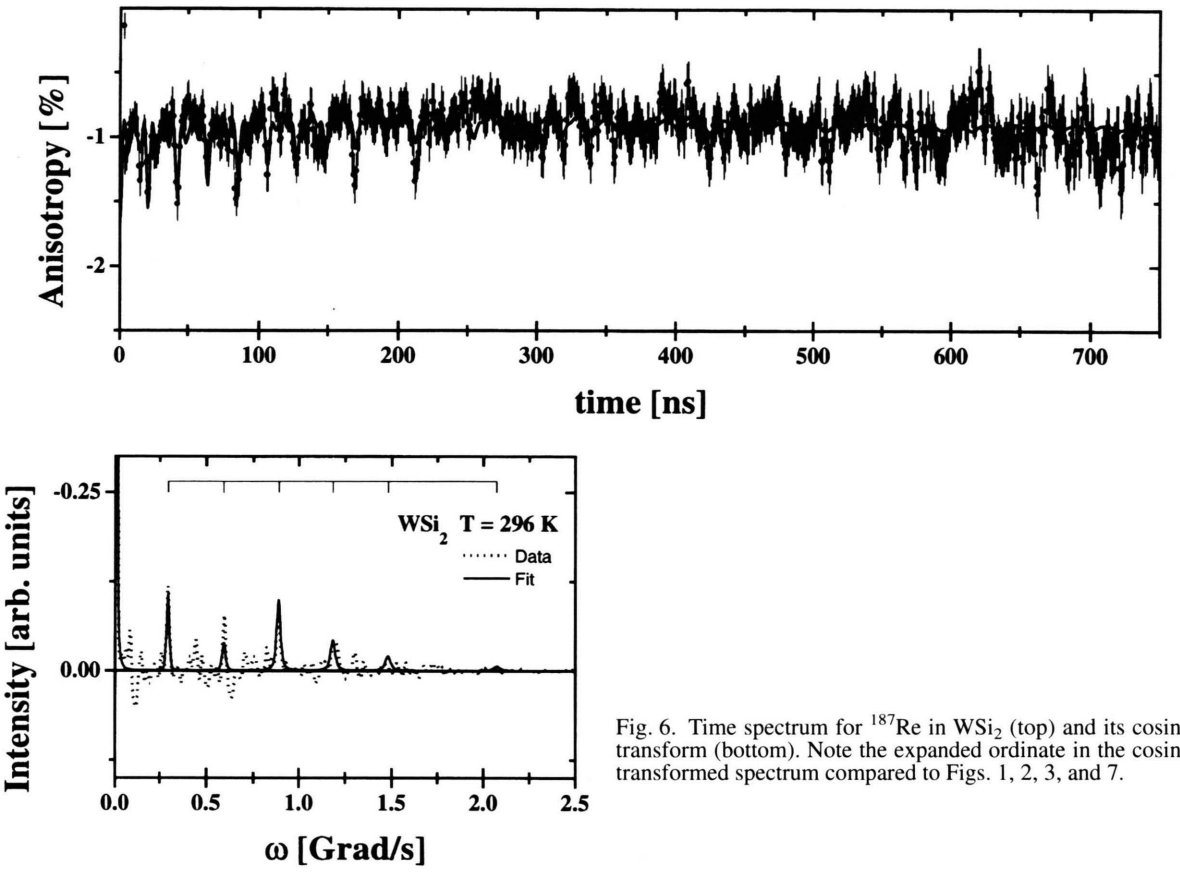

Fig. 6. Time spectrum for ^{187}Re in WSi_2 (top) and its cosine transform (bottom). Note the expanded ordinate in the cosine transformed spectrum compared to Figs. 1, 2, 3, and 7.

at 911 K is unclear. It certainly is not due to pile up (see the other spectra in Figure 8) because we always used about the same source strength. It rather might be indicative for the beginning of thermal decomposition. The fit results are summarized in Table 3, ν_Q versus temperature is displayed in Fig. 5, and the fit parameters according to (10) are listed in Table 2.

Table 3. Summary of fit results for ^{187}Re in $CaWO_4$ at various temperatures.

T	ω_1	Amplitude	δ	η	ν_Q	$\lvert V_{zz}\rvert$
[K]	[Mrad/s]	[%]	[%]		[MHz]	[10^{21} V/m^2]
296	284.30(2)	−1.19(3)	0.00	0.00	1085.9(1)	14.8(2)
453	281.98(6)	−1.14(7)	0.00	0.00	1077.1(2)	14.7(2)
629	277.59(4)	−1.22(6)	0.00	0.00	1060.3(2)	14.4(2)
767	273.64(7)	−0.76(6)	0.00	0.00	1045.2(2)	14.2(2)
911	267.61(5)	−1.61(9)	0.00	0.00	1022.2(2)	13.9(2)

5.2. Ab-initio Calculations of Electric Field Gradients

Calculations of electron densities and electric field gradients were carried out using the full potential linearized augmented plane wave (FLAPW) method as embodied in the program package WIEN95 [19]. The method is based on crystal periodicity. Because the TDPAC-measurements were carried out at Re-atoms due to the $^{187}W(\beta^-)^{187}Re$ transmutation, we had to consider Re impurities within the ideal crystal. We carried out the following three types of calculations:

(i) pure compound, unit cell,
(ii) pure compound, artificial supercell comprising many unit cells. This was done to facilitate comparison with
(iii) impurity system (Re at central W-site), supercell.

In particular we used the supercells listed in Table 4. Generally, we had one Re atom per seven W atoms. For WS_2, WSe_2, and WSi_2 we doubled the unit cell in the *a*- and *b*-directions only because in the *c*-direction there

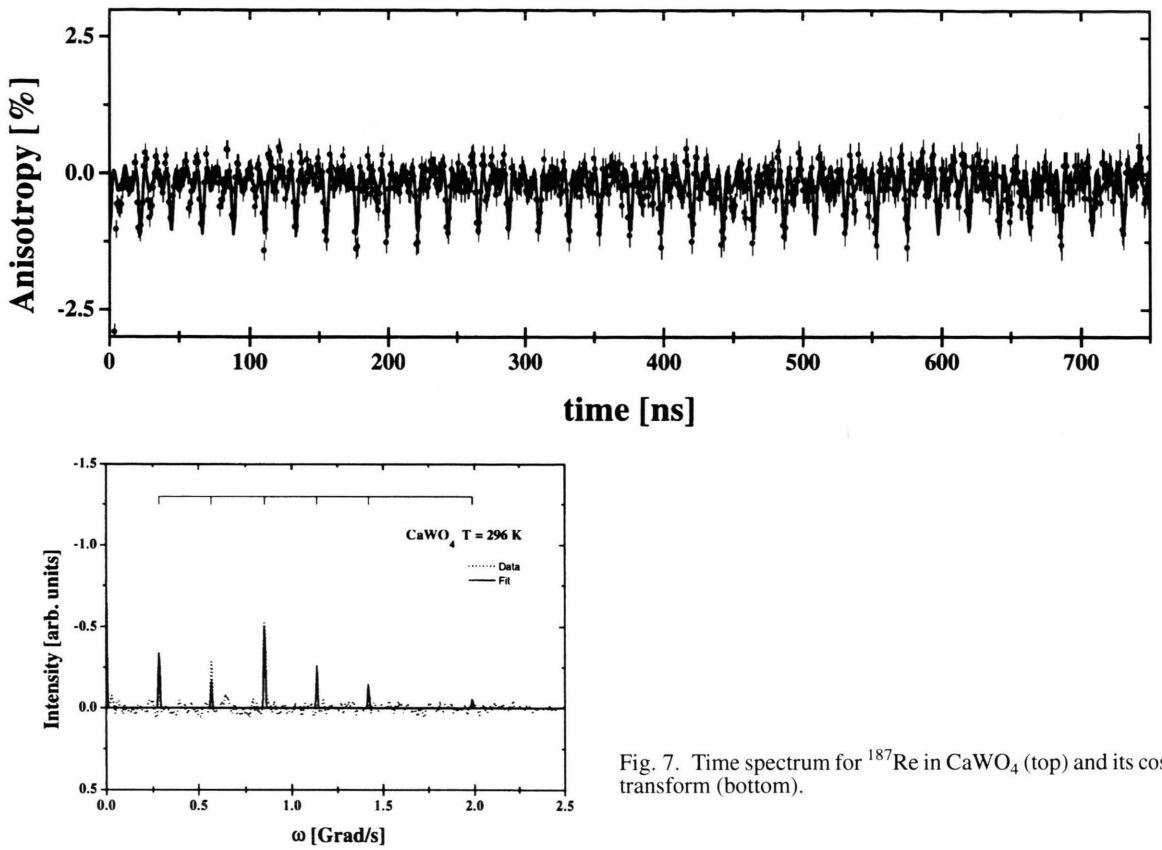

Fig. 7. Time spectrum for ^{187}Re in $CaWO_4$ (top) and its cosine transform (bottom).

Table 4. Size of used supercells in units of the unit cell dimensions and ratio of impurity (Re) atoms to W-atoms.

Compound	$a^{\text{supercell}}$	$c^{\text{supercell}}$	Ratio Re:W
WC	$2a$	$2c$	1:7
	$3a$	$3c$	1:27
WS_2, WSe_2, WSi_2	$2a$	$1c$	1:7
$CaWO_4$	No supercell calculations performed.		

are two layers of W-atoms separated by two layers of S, Se, or Si, respectively, within one unit cell. We replaced one W-atom in one of the layers. In the case of WC we had to double the unit cell in the c-direction, too. Due to the small unit cell of WC, a supercell composed of $3 \times 3 \times 3$ unit cells could also be tested leading to an impurity to W ratio of 1:27. However, in this case no full convergence of the basis set could be reached due to main memory limitations. Furthermore, we investigated a hypothetical "ReC", assuming the same crystal structure and unit cell dimensions as for WC. The unit cell of $CaWO_4$ is too large, and so we did not perform supercell calculations yet.

We checked several convergence parameters. With the exception of $CaWO_4$, the treatment of the systems with standard unit cells needed only small plane wave basis sets due to small unit cells. We used an extended number of $\boldsymbol{k}$-points (at least 100) in the irreducible wedge of the Brillouin zone. For most of the supercells, about 10 $\boldsymbol{k}$-points were used and plane wave basis set convergence could also be reached. The CPU time per iteration was about two days for the supercells and a few minutes for the standard unit cells on a HP 9000/780 computer.

In Table 5 the results for V_{zz} and η at the central W and Re positions, respectively, are listed for the standard unit cell and supercell calculations. In principle, the results for single unit cells and the supercells without impurity should be the same, but due to different basis sets and $\boldsymbol{k}$-meshes small differences occurred, indicating the accuracy limits of such calculations. Larger differences occurred between the single unit cell and the 1:27 unit cell for WC. This is due to the fact that for the large super-

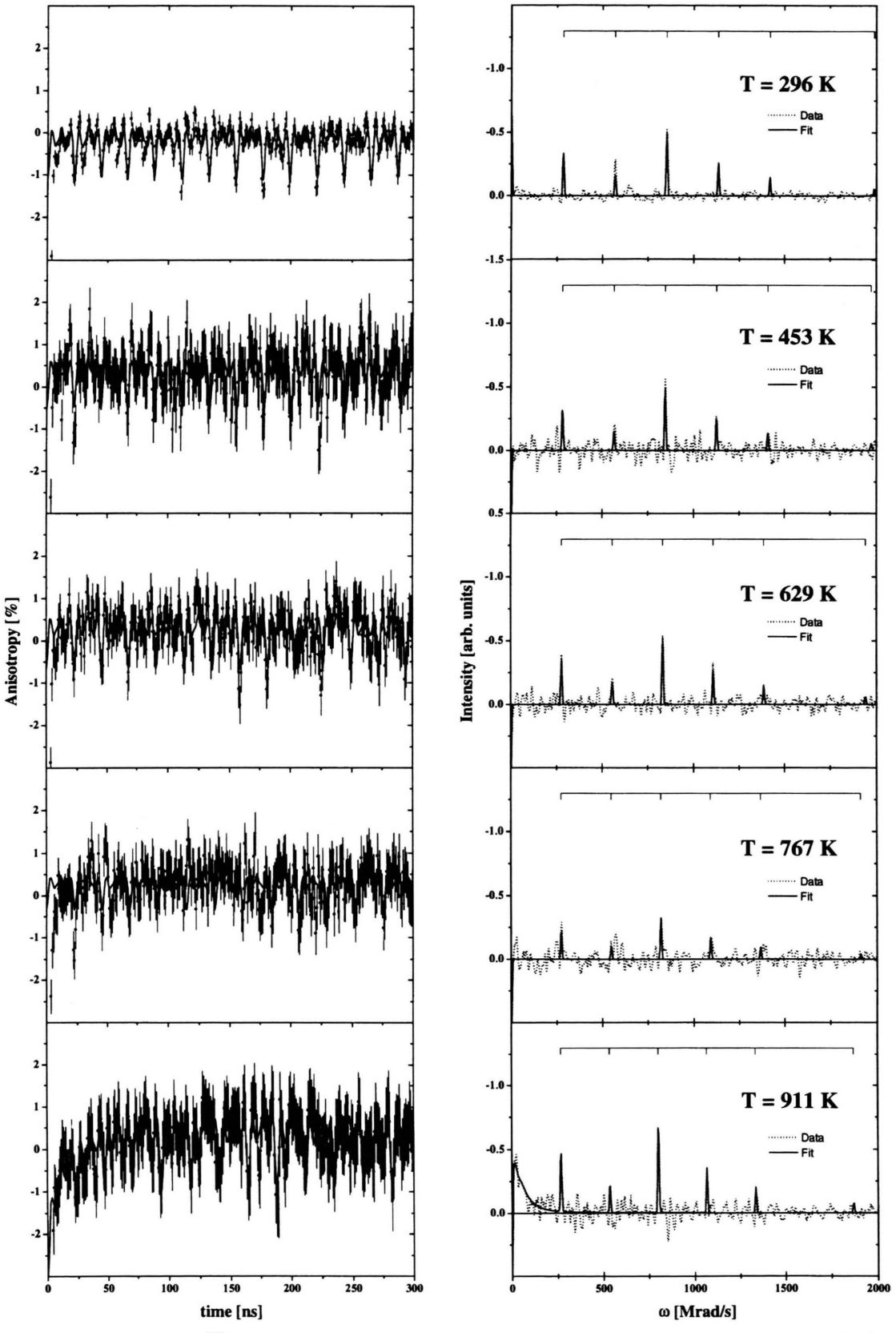

Fig. 8. Time spectrum for ^{187}Re in $CaWO_4$ (left) and their cosine transforms (right) at various temperatures. In the time spectra the first 300 ns are shown only.

Table 5. Supercell calculations of EFGs for atomic sites in WC (unit cell and supercell), Re in WC, "ReC" (unit cell), $CaWO_4$, WS_2, Re in WS_2, WSe_2, Re in WSe_2, WSi_2, and Re in WSi_2.

Compound	Cell	Atom	Number	Position	$R_{impurity-atom}$ [a.u.[a]]	V_{zz} [10^{21} V/m^2]	η
WC	single unit cell	W	1	(0, 0, 0)	0.000	–13.60	0.000
		C	1	$(\frac{2}{3}, \frac{1}{3}, \frac{1}{2})$	4.152	–0.13	0.000
WC	supercell 1:7	W	1	(0, 0, 0)	0.000	–14.50	0.000
	without impurity[b]	C	6	$(\frac{1}{3}, \frac{1}{6}, \frac{1}{4})$	4.152	–0.12	0.000
WC	supercell 1:27 without impurity[c]	W	1	(0, 0, 0)	0.000	–8.4	0.000
WC	supercell 1:7	Re	1	(0, 0, 0)	0.000	–5.70	0.000
	with Re impurity	C	6	$(\frac{1}{3}, \frac{1}{6}, \frac{1}{4})$	4.152	0.62	0.153
		W	1	$(0, 0, \frac{1}{2})$	5.360	–4.18	0.000
		W	3	$(0, \frac{1}{2}, 0)$	5.492	–16.40	0.558
		C	2	$(\frac{1}{3}, \frac{2}{3}, \frac{1}{4})$	6.885	–0.19	0.000
		W	3	$(0, \frac{1}{2}, \frac{1}{2})$	7.675	–10.77	0.046
WC	supercell 1:27 with Re impurity	Re	1	(0, 0, 0)	0.000	–5.5	0.000
"ReC"	same structure as	Re	1	(0, 0, 0)	0.000	–6.50	0.000
	WC	C	1	$(\frac{2}{3}, \frac{1}{3}, \frac{1}{2})$	4.152	–0.13	0.000
WS_2	single unit cell	W	2	$(\frac{1}{3}, \frac{2}{3}, \frac{1}{4})$	0.000	–18.60	0.000
		S	4	$(\frac{1}{3}, \frac{2}{3}, 0.6225)$	4.547	–4.70	0.000
WS_2	supercell 1:7	W	1	$(\frac{1}{6}, \frac{1}{3}, \frac{1}{4})$	0.000	–18.05	0.000
	without impurity[b]	S	3	$(\frac{5}{6}, \frac{1}{6}, (0.1225)$	4.547	–4.52	0.000
WS_2	supercell 1:7	Re	1	$(\frac{1}{6}, \frac{1}{3}, \frac{1}{4})$	0.000	–14.64	0.000
	with Re impurity	S	3	$(\frac{5}{6}, \frac{1}{6}, 0.1225)$	4.547	–5.24	0.792
		S	3	$(\frac{5}{6}, \frac{1}{6}, 0.3775)$	4.547	–5.24	0.792
		W	3	$(\frac{1}{6}, \frac{5}{6}, \frac{1}{4})$	5.959	–19.80	0.311
		S	1	$(\frac{5}{6}, \frac{2}{3}, 0.1225)$	7.496	–4.87	0.000
		S	1	$(\frac{5}{6}, \frac{2}{3}, 0.3775)$	7.496	–4.87	0.000
		S	1	$(\frac{1}{6}, \frac{1}{3}, 0.6225)$	8.688	–4.46	0.000
		S	1	$(\frac{1}{6}, \frac{1}{3}, 0.8775)$	8.688	–4.46	0.000
		S	3	$(\frac{1}{6}, \frac{5}{6}, 0.6225)$	10.524	–4.40	0.018
		S	3	$(\frac{1}{6}, \frac{5}{6}, 0.8775)$	10.542	–4.40	0.018
		W	3	$(\frac{5}{6}, \frac{1}{6}, \frac{3}{4})$	12.141	–17.90	0.000
		W	1	$(\frac{5}{6}, \frac{2}{3}, \frac{3}{4})$	13.524	–17.55	0.000
WSe_2	single unit cell	W	2	$(\frac{1}{3}, \frac{2}{3}, \frac{1}{4})$	0.000	–15.20	0.000
		Se	4	$(\frac{1}{3}, \frac{2}{3}, 0.6211)$	4.547	–6.10	0.000

Table 5. Continued from previous page.

Compound	Cell	Atom	Number	Position	$R_{impurity-atom}$ [a.u.[a]]	V_{zz} [10^{21} V/m^2]	η
WSe_2	supercell 1:7	W	1	$(\frac{1}{6}, \frac{1}{3}, \frac{1}{4})$	0.000	−14.65	0.000
	without impurity	Se	3	$(\frac{5}{6}, \frac{1}{6}, 0.1211)$	4.774	−6.79	0.083
		Se	3	$(\frac{5}{6}, \frac{1}{6}, 0.3789)$	4.774	−6.79	0.083
		W	3	$(\frac{1}{6}, \frac{5}{6}, \frac{1}{4})$	6.202	−14.55	0.027
		Se	1	$(\frac{5}{6}, \frac{2}{3}, 0.1211)$	7.826	−6.76	0.000
		Se	1	$(\frac{5}{6}, \frac{2}{3}, 0.3789)$	7.826	−6.76	0.000
		Se	1	$(\frac{1}{6}, \frac{1}{3}, 0.6211)$	9.089	−6.76	0.000
		Se	1	$(\frac{1}{6}, \frac{1}{3}, 0.8789)$	9.089	−6.76	0.000
		Se	3	$(\frac{1}{6}, \frac{5}{6}, 0.6211)$	11.003	−6.79	0.083
		Se	3	$(\frac{1}{6}, \frac{5}{6}, 0.8789)$	11.003	−6.79	0.083
		W	3	$(\frac{5}{6}, \frac{1}{6}, \frac{3}{4})$	12.758	−14.55	0.027
		W	1	$(\frac{5}{6}, \frac{2}{3}, \frac{3}{4})$	14.186	−14.65	0.000
WSe_2	supercell 1:7 with	Re	1	$(\frac{1}{6}, \frac{1}{3}, \frac{1}{4})$	0.000	−14.88	0.000
	Re impurity	Se	3	$(\frac{5}{6}, \frac{1}{6}, 0.1211)$	4.774	−9.55	0.936
		Se	3	$(\frac{5}{6}, \frac{1}{6}, 0.3789)$	4.774	−9.55	0.936
		W	3	$(\frac{1}{6}, \frac{5}{6}, \frac{1}{4})$	6.202	−19.21	0.292
		Se	1	$(\frac{5}{6}, \frac{2}{3}, 0.1211)$	7.826	−8.56	0.000
		Se	1	$(\frac{5}{6}, \frac{2}{3}, 0.3789)$	7.826	−8.56	0.000
		Se	1	$(\frac{1}{6}, \frac{1}{3}, 0.6211)$	9.089	−7.64	0.000
		Se	1	$(\frac{1}{6}, \frac{1}{3}, 0.8789)$	9.089	−7.64	0.000
		Se	3	$(\frac{1}{6}, \frac{5}{6}, 0.6211)$	11.003	−7.51	0.021
		Se	3	$(\frac{1}{6}, \frac{5}{6}, 0.8789)$	11.003	−7.51	0.021
		W	3	$(\frac{5}{6}, \frac{1}{6}, \frac{3}{4})$	12.758	−17.44	0.011
		W	1	$(\frac{5}{6}, \frac{2}{3}, \frac{3}{4})$	14.186	−17.12	0.000
WSi_2	single unit cell	W	2	(0, 0, 0)	0.000	−15.00	0.000
		Si	4	(0, 0, 0.3345)	4.956	−0.70	0.000
WSi_2	supercell 1:7	W	1	(0, 0, 0)	0.000	−14.83	0.000
	without impurity	Si	2	$(\frac{3}{4}, \frac{3}{4}, 0.8345)$	4.950	−1.01	0.005
		Si	2	$(\frac{1}{4}, \frac{1}{4}, 0.8345)$	4.950	−1.00	0.005
		Si	4	$(\frac{1}{4}, \frac{3}{4}, 0.8345)$	4.950	−1.01	0.009
		Si	2	(0, 0, 0.3345)	4.956	−1.00	0.005
		W	2	$(\frac{1}{2}, 0, 0)$	6.081	−15.10	0.002

Table 5. Continued from previous page.

Compound	Cell	Atom	Number	Position	$R_{impurity-atom}$ [a.u.[a]]	V_{zz} [10^{21} V/m^2]	η
		Si	4	$(\frac{1}{2}, 0, 0.3345)$	7.846	−1.01	0.009
		W	1	$(\frac{1}{4}, \frac{1}{4}, \frac{1}{2})$	8.565	−14.83	0.000
		W	1	$(\frac{3}{4}, \frac{3}{4}, \frac{1}{2})$	8.565	−15.10	0.000
		W	2	$(\frac{3}{4}, \frac{1}{4}, \frac{1}{2})$	8.565	−15.10	0.002
		W	1	$(\frac{1}{2}, \frac{1}{2}, 0)$	8.600	−15.10	0.000
		Si	2	$(\frac{1}{2}, \frac{1}{2}, 0.3445)$	9.925	−1.01	0.005
WSi_2	supercell 1:7 with Re impurity	Re	1	(0, 0, 0)	0.000	−18.54	0.000
		Si	2	$(\frac{3}{4}, \frac{3}{4}, 0.8345)$	4.950	−1.31	0.856
		Si	2	$(\frac{1}{4}, \frac{1}{4}, 0.8345)$	4.950	−1.32	0.852
		Si	4	$(\frac{1}{4}, \frac{3}{4}, 0.8345)$	4.950	−1.32	0.850
		Si	2	(0, 0, 0.3345)	4.956	−0.14	0.824
		W	2	$(\frac{1}{2}, 0, 0)$	6.081	−22.17	0.435
		Si	4	$(\frac{1}{2}, 0, 0.3345)$	7.846	−1.11	0.022
		W	1	$(\frac{1}{4}, \frac{1}{4}, \frac{1}{2})$	8.565	−14.57	0.061
		W	1	$(\frac{3}{4}, \frac{3}{4}, \frac{1}{2})$	8.565	−14.69	0.059
		W	2	$(\frac{3}{4}, \frac{1}{4}, \frac{1}{2})$	8.565	−14.76	0.059
		W	1	$(\frac{1}{2}, \frac{1}{2}, 0)$	8.600	−19.54	0.002
		Si	2	$(\frac{1}{2}, \frac{1}{2}, 0.3345)$	9.925	−0.93	0.114
$CaWO_4$	single unit cell	W	4	$(0, \frac{1}{4}, \frac{1}{8})$	0.000	+15.0	0.000

[a] Atomic unit. 1 a.u. = $5.29177 \cdot 10^{-11}$ m.

[b] Within the quoted accuracy, all values for V_{zz} and η on W and non-metal sites turned out to be identical.

[c] One $\boldsymbol{k}$-point only!

cell no full convergence of the plane wave basis set could be reached and only one $\boldsymbol{k}$-point was used for computational reasons.

In Table 5, also the values for V_{zz} and η for the other atoms in the pure and impurity systems are given. It is interesting to see that V_{zz}, η-values at inequivalent lattice sites in the artificial supercells – which, however, are of course equivalent in the unit cell – turn out to be identical within the quoted accuracy, the cases of WSe_2 and WSi_2 being slightly less accurate. Note, that the nearest and next nearest neighbours of the Re impurity exhibit V_{zz}, η-parameters vastly different from the pure systems.

We investigated the forces on the atoms. In the case of the systems without impurity the forces were nearly zero and no structure relaxation was necessary. In the case of the supercells we found forces of the order of 10 mRy/a.u. at the nearest neighbours of the Re atom. Due to the excessive computing time reqirements we performed relaxations for the 1:7 supercell of WC only. In this case, where Re and W have similar size and chemical properties, the change of V_{zz} is in the order of the ba-

Table 6. Calculated and experimental values for V_{zz} and η at various lattice sites. Note that it is in principle not possible to determine the sign of V_{zz} by γ-γ-TDPAC.

	LAPW (calc.)		Mössbauer (exp.)	TDPAC (exp.)
	V_{zz}^{W} [10^{21} V/m^2]	V_{zz}^{Re} [10^{21} V/m^2]	V_{zz}^{W} [10^{21} V/m^2]	V_{zz}^{Re} [10^{21} V/m^2]
WC	−13.6	−5.7	−12.1 ($\eta = 0.52$)	±4.6(2)
WS_2	−18.6	−14.6	−18.6(5)	±14.9(2)
WSe_2	−15.2	−14.9		±14.0(2)
WSi_2	−15.0	−18.5		±15.4(2)
$CaWO_4$	+15			±14.8(2)

sis set effects (less than 10%). Therefore a good basis set is more important than very time consuming calculations of small relaxation effects.

In Table 6 the most accurate calculated values are compared with the experimental values.

6. Discussion

6.1. *Effective Anisotropy* A_{22}^{eff}

The observed values of A_{22}^{eff} (–1...–2%) are rather low compared to the calculated value of $A_{22} = -13.1\%$ for the 479.5 keV – 72 keV cascade (assuming pure multipolarities). Unperturbed angular correlation experiments with solid state detectors and excellent energy resolution confirmed [20] that the γ-transitions are essentially of pure E2 and E1 character. There are two main reasons for the reduction of A_{22}:

(i) Solid angle correction factors $Q_2(\gamma_1)$ $Q_2(\gamma_2)$ average partly over $P_2(\cos\theta)$ due to the finite acceptance. We have no accurate values for the Q_2's for our conically scintillators, but experience with other isotopes, e.g. ^{181}Hf, tells us that for the rather short source-detector distances of 5–10 mm we should have $Q_{22} = 0.5$ in the worst cases [11].

(ii) The admixture of X-rays in the stop channel (72 keV) which is practically isotropic in coincidence with the 479.5 keV-line is considered the main reason for the further reduction of A_{22} by at least another factor of 2. With NaI(Tl) scintillators $A_{22}^{\text{eff}} = -7\%$ (corrected for Q_{22}) was observed, whereas BaF_2-scintillators with a poorer energy resolution are doing much worse. We plan to cool our BaF_2-scintillators in order to achieve a better energy resolution (aim: $\Delta E/E = 10\%$ at 662 keV). This would greatly help to increase A_{22}^{eff}.

Another trivial reason for the low A_{22}^{eff} would be the fact that fraction of probe nuclei on regular lattice sites without neighbouring or more distant defects would give rise to a sharp NQI-signal, while all other probe nuclei associated with lattice defects merely give a rather broad frequency distribution with a very rapid decay of the anisotropy which might be hidden under the huge prompt contribution. This possibility can be ruled out because we should observe an increase of A_{22}^{eff} during annealing, which was not the case. In addition, our prompt peak would masquerade a rapid decay of the anisotropy for 1–5 ns only, and there is no reason that all defect associated signals are so much higher in frequency than the regular signals. In order to clarify this point further, we plan experiments with ^{187}W of extremely high specific activity, i.e. with low X-ray fluorescence probability.

6.2. *Linewidth*

The linewidth, assumed Lorentzian, was very small or even zero in all cases where the sample quality was checked by other techniques (e.g. STM for the layered dichalcogenides, or EPR for Na-doped $CaWO_4$). It was relatively high for WC and WSi_2, two compounds purchased commercially and checked for purity only. Apparently, the crystal quality of these polycrystalline substances is inferior to that of the single crystalline materials mentioned above. In principle, the linewidth could be the result of distant lattice defects (not correlated with the thermal neutron capture producing the ^{187}W probe), produced e.g. by fast neutrons. Since we did not observe a significant line narrowing upon annealing, we rule out this possibility. In cases with $\delta = 0$ we expect to improve the frequency resolution by a factor of 4 by observing coincidences up to 3 μs.

6.3. *NQI-Parameters at Room Temperature*

The observation of axial symmetry ($\eta = 0$) is not surprising for the compounds studied due to the symmetry of their crystal structures.

It is little surprising that all NQI-frequencies are very roughly the same with the exception of WC. It looks as if the EFG at Re impurities in W-compounds is dominated by impurity specific contributions which would render the "fingerprint" method with this isotope useless. However, we believe that this coincidence is fortuitous. Clearly, the results for WS_2 and WSe_2 are expected to be similar because of the similarity of both structures. It is interesting to note that ν_Q for WSe_2 is slightly lower compared to WS_2, contrary to the case of ^{181}Ta in 2H-TaS_2 and 2H-$TaSe_2$ at room temperature ($\omega = 820$ Mrad/s and 870 Mrad/s, respectively) [21]. This might be an impurity specific effect (see also below). The result for WSi_2 is difficult to interpret because of the lack of comparative data. Inspection of Table 6 shows that the sign of V_{zz} in $CaWO_4$ at W-sites is opposite to that of all other compounds where calculations were performed. Hence, the coincidence of the magnitude of V_{zz} with those of the other compounds is indeed fortuitous.

The agreement between the experimental values for $|V_{zz}|$ at Re impurities on W-sites and the calculated V_{zz} is excellent for WC, WS_2, WSe_2, and WSi_2, especially taking into account that the FPLAPW-method is not designed to investigate impurities and the ratio between impurity and W atoms is large compared to the experimental case. Obviously, the influence of the periodically continued impurities is rather small. This is supported by the small difference between V_{zz} at a Re impurity in WC and at Re in the hypothetic "ReC". In fact, it is more important to improve the basis set than to increase the unit cell by more than a factor of two in all directions, as was done for WC, which led to a worse basis set.

The agreement between theory and experiment is even perfect for WS_2 when Mössbauer-data [22] for W-sites are considered. The fact that the EFG at Re impurities in WS_2 is smaller by 20% compared to that at a W-site might be considered an impurity specific effect. We do not think that a discussion in terms of Sternheimer factor differences [23] is meaningful. We find an increasing Re EFG with respect to the W EFG in WSi_2, an almost constant one in WSe_2, and decreasing values in WS_2 and WC, despite the fact that the Sternheimer factor would predict the same tendency for all investigated compounds.

The calculated value for V_{zz} at W-sites in WC is relatively high ($V_{zz} = -13.6 \cdot 10^{21}$ V/m^2), comparable to that obtained by Mössbauer spectroscopy[5] ($-12.1 \cdot 10^{21}$ V/m^2) [24]. The experimental result at ^{187}Re is lower by a factor of roughly 3 compared to the W-site. Hence, the electronic charge distribution around the impurity is very different from that of a regular W-site. This is also shown by the EFG-calculations: The EFG is much smaller at Re impurities, with and without lattice relaxation. It is interesting to note in this context that WC is the only compound where the R-analogue does not exist [25][6]. Hence, the Re impurity is "trapped" at an "unfavourable" W-site after nuclear transmutation.

6.4. *Temperature Dependence of* ν_Q

Inspection of Table 2 shows that $\nu_Q(T)$ closely follows a $T^{3/2}$-behaviour for WS_2 and WSe_2, contrary to what is known from other layered transition metal dichalcogenides like 2H-TaS_2 [21], 2H-$TaSe_2$ [21], and 2H-$NbSe_2$ [26] with a linear temperature dependence over extended temperature ranges. The logarithmic temperature derivatives at 300 K, however, compare well. We have (in units of 10^{-4} K^{-1}): -1.2 (2H-WS_2), -1.0 (2H-WSe_2), -1.4 (2H-TaS_2), -1.3 (2H-$TaSe_2$), -2.1 (2H-$NbSe_2$). It is interesting to note that the temperature derivatives for the selenides are a little bit smaller than those for the sulfides, possibly an effect of the higher mass of Se. The deviation from a linear temperature dependence, which was analyzed and explained by Torgeson and Borsa [26] to be a result of anharmonic lattice vibrations, is more difficult to explain. First, the original theory of Jena [27] was restricted to metals and is not applicable to large bandgap semiconductors. Second, we must not forget the impurity specific effects which might be superimposed onto those of the regular lattice. Curiously enough, a $T^{3/2}$-temperature dependence was observed for many 3-dimensional (~isotropic) metals [28]. A wider temperature range, particularly below 300 K, should be considered before drawing any further conclusions.

The situation is different for $CaWO_4$: Here, the temperature exponent is larger (2.2) while the prefactor is at least two orders of magnitude lower compared to the layered dichalcogenides. The room temperature logarithmic derivative is small: $\left(\frac{d \ln \nu_Q}{dT}\right)_{300\,K} = -0.5 \cdot 10^{-4}$ K^{-1}. Again, no further conclusions should be drawn without low-temperature data.

7. Summary

Despite a number of technical problems – part of which were solved during this study, others have yet to be cured – it is clear that the nuclear TDPAC-probe $^{187}W(\beta^{-P})$ ^{187}Re is extremely well suited for NQI-studies. The extraordinary frequency resolution of $\Delta\omega/\omega$, reaching values of 0.3% around 1 Grad/s (which can readily be improved to below 0.1%), offers a very sensitive means to detect dynamical broadening due to molecular tumbling in solution or due to intramolecular reorientational motion in W-containing macromolecules. Fast scintillators with greatly improved energy resolution would boost the application of this isotope in material sciences as well as life sciences. Finally, ab initio calculations of EFG's and impurity specific effects will help to go beyond a "fingerprint" identification of compounds.

[5] The authors of [24] assumed $\eta = 0.52$ in their data analysis. We believe that the material used was not single phase. It is difficult to estimate the extent of changes in the derived V_{zz} if $\eta = 0$ were used in the data analysis.

[6] The Re-analoguous of WS_2, WSe_2, WSi_2, and $CaWO_4$ do exist, albeit with slightly modified (distorted) structures.

Acknowledgement

It is a great pleasure to thank the team of the Forschungsreaktor München, especially Dr. U. Wagner and J. E. Punsch, for helping to carry out the irradiation of the samples.

We are very grateful to Prof. F. Lévy, Prof. E. Bucher, Prof. G. Völkel, and Dr. J. Simon for providing WS_2, WSe_2, and $CaWO_4$ single crystals.

[1] E. Furimsky. Catal. Rev. Sci. Engl **22**, 371 (1980).
[2] H. Knözinger. In M. Phillips and M. Ternan (eds.), Proceedings of the 9th International Congress on Catalysis, Vol. 5, P. 20, Calgary, 1989. The Chemical Institute of Canada, Ottawa.
[3] P. Høglikøj and F. E. Christensen. 1994 Structures Technical Digest, Physics of X-Ray-Multilayers, p 159–162. Number 6 in Technical Digest Series. Optical Society of America, Jackson Hole 1994.
[4] R. A. Schmitz, M. Richter, D. Linder, and R. K. Thauer. Eur. J. Biochem. **207**, 559 (1992).
[5] R. A. Schmitz, S. P. J. Albracht, and R. K. Thauer. Eur. J. Biochem. **209**, 1013 (1992).
[6] P. A. Bertram, R. A. Schmitz, D. Linder, and R. K. Thauer. Arch. Microbiol. **161**, 220 (1994).
[7] T. Butz. Nuclear quadrupole interactions studied by time differential perturbed angular correlation of γ-rays. In G. Wulfsberg and R. Marino (eds.), Proceedings of the XIIIth International Symposium on NQI Spectroscopy, p. 396–410, Providence Rhode Island, USA, 1996. Verlag Z. Naturforsch. Tübingen.
[8] J. G. Roper and H. B. Knowles. Physics Letters, **38A**, 477 (1972).
[9] H. Haas and D. A. Shirley. J. Chem. Phys. **58**, 3339 (1973).
[10] P. Mottner and T. Butz. Chem. Physics **147**, 199 (1990).
[11] T. Butz, S. Saibene, Th. Fraenzke, and M. Weber. Nucl. Instr. Meth. **A284**, 417 (1989).
[12] T. Butz, M. Ceolín, P. Ganal, P. Schmidt, M. A. Taylor, and W. Tröger. Physica Scripta **54**, 234 (1996).
[13] J. Leciejewicz. Acta Crystallographica **14**, 200 (1961).
[14] W. J. Schutte, J. L. De Boer, and F. Jellinek. J. Solid State Chem. **70**, 207 (1987).
[15] O. Glemser, H. Sauer, and P. König. Z. Anorg. Allgem. Chem. **257**, 241 (1948).
[16] A. N. Christensen. J. Crystal Growth **129**, 266 (1993).
[17] R. M. Hazen, L. W. Finger, and J. W. E. Mariathasan. J. Phys. Chem. Solids **46**, 253 (1985).
[18] J. C. I. Bailar and A. F. Trothman-Dickenson (eds.). Compendium Publishers, 1st edition, Fairway Park, Elmsford, New York 1973.
[19] P. Blaha, K. Schwarz, P. Sorantin, and S.B. Trickey. Comput. Phys. Commun. **59**, 399 (1990). Updated WIEN95 version was used.
[20] Nuclear Data Sheet **36**, 559, August 1982.
[21] M. Naito, H. Nishihava, and T. Butz. In T. Butz (ed.), Nuclear Spectroscopy on Charge Density Wave Systems, Kluwer Academic Publ., Dordrecht 1992, p 35–106.
[22] D. Agresti, E. Kankeleit, and B. Persson. Phys. Rev. **155**, 1342 (1967).
[23] F. D. Feiock and W. R. Johnson. Phys. Rev. **187**, 39 (1969).
[24] A. Gedikli, H. Winkler, and E. Gerdau. Z. Physik **267**, 61 (1974).
[25] Fachinformationszentrum Karlsruhe and Gmelin-Institut für anorganische Chemie, Frankfurt. Inorganic Crystal Structure Data Base.
[26] D. R. Torgeson and F. Borsa. Phys. Rev. Letters **37**, 956 (1976).
[27] P. Jena. Phys. Rev. Letters **36**, 418 (1976).
[28] J. Christiansen, P. Heubes, R. Keitel, W. Klinger, W. Loeffler, W. Sandner, and W. Witthuhn. Z. Physik **B24**, 177 (1976).